Inorganic Chemistry
Article
pubs.acs.org/IC

Magic-Size II−VI Nanoclusters as Synthons for Flat Colloidal Nanocrystals

Yuanyuan Wang, Yang Zhou, Ying Zhang, and William E. Buhro*

Department of Chemistry, Washington University, St. Louis, Missouri 63130-4899, United States

Ⓢ *Supporting Information*

ABSTRACT: Five new, discretely sized, magic-size II−VI nanoclusters are synthesized in primary-amine bilayer templates and are isolated as the derivatives [(CdS)$_{34}$(*n*-butylamine)$_{18}$], [(ZnS)$_{34}$(*n*-butylamine)$_{34}$], [(ZnSe)$_{13}$(*n*-butylamine)$_{13}$], [(CdTe)$_{13}$(*n*-propylamine)$_{13}$], and [(ZnTe)$_{13}$(*n*-butylamine)$_{13}$]. The nanoclusters are characterized by elemental analysis, UV−visible absorption spectroscopy, laser-desorption-ionization mass spectrometry, and transmission electron microscopy. Four of the nanocluster precursors are converted to wurtzitic CdS, ZnS, and ZnSe quantum platelets and CdTe quantum belts, respectively, under mild conditions.

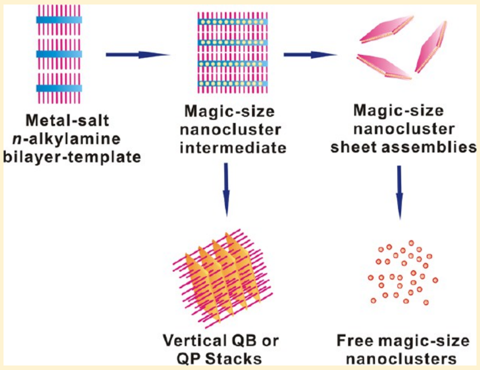

■ INTRODUCTION

We describe herein the isolation of several primary-amine derivatives of magic-size nanoclusters of the semiconductors CdS, ZnS, ZnSe, CdTe, and ZnTe. Their precise stoichiometries are established by a combination of absorption spectroscopy, mass spectrometry, and elemental analysis. The magic-size nanoclusters are grown within spontaneously formed, lamellar, amine-bilayer mesophases. They are converted into flat, colloidal nanocrystals of the corresponding II−VI semiconductors while entrained within these lamellar template structures.

Clusters composed of main-group elements have fascinated inorganic chemists since the structures of the polyhedral boranes were discovered in the 1950s.[1] Main-group cluster chemistry developed rapidly in that era with expansion of the carborane,[2] metallaborane,[3] and metallacarborane[2] fields, in which the clusters exhibited analogous deltahedral structures and conformed to the same skeletal-electron-counting principles.[4]

The Zintl-anion clusters composed of Sn, Ge, Pb, Bi, Sb, and their combinations subsequently joined these families of deltahedral clusters.[5] Corbett provided a major advance in the chemistry of Zintl anions by sequestering their counter-cations within 2,2,2-crypt, stabilizing the clusters against back electron transfer.[6] The stabilized cluster compounds were isolated in crystalline form, allowing Corbett and co-workers to obtain the first X-ray structural characterizations of Zintl-anion clusters.

Discrete molecular clusters of elemental carbon were first isolated by Kräetschmer et al. in 1990,[7] resulting in the dramatic growth of the carbon-fullerene field at that time. The C_{60} and C_{70} clusters are the best-known and most-stable fullerenes, although the even-numbered carbon clusters larger than C_{32} are stable.[8] As is well-known, the structures of these clusters consist of hollow cages constructed by the fusion of five- and six-membered rings. The field has expanded to include endohedral metallofullerenes having atoms, molecules, or clusters encapsulated within the fullerene cages[9] and heterofullerenes having heteroatom substitutions of cage carbon atoms.[10]

A newly emergent family of main-group clusters consists of the so-called magic-size nanoclusters of CdSe, $(\mathrm{CdSe})_x$ where x = 13, 19, 33, 34, etc., and their II−VI congeners.[11] Magic-size nanoclusters were first detected in the early II−VI nanoparticle research of Henglein and co-workers in the 1980s.[12] They were suggested to be small, discretely sized clusters by their blue-shifted and comparatively sharp absorption spectra relative to those of the larger nanoparticles. Magic-size nanocluster spectral features have been observed frequently in the early stages of nanocrystal synthesis since that time.[11g,13,14] In an important study, Manna and co-workers demonstrated that the spectra of magic-size CdSe nanoclusters evolve in discrete rather than continuous shifts as the nanoclusters grow from one discrete, stable size to the next.[11a]

The precise stoichiometries and structures of these II−VI nanoclusters remain to be fully resolved. The crystallographically characterized examples that have been isolated from solution syntheses exhibit *nonstoichiometric* (non 1:1) II−VI compositions and close-packed zinc blende or wurtzite core structures.[15] These nanoclusters also contain anionic ligands to charge balance the nonstoichiometric II−VI compositions.

Special Issue: To Honor the Memory of Prof. John D. Corbett

Received: November 3, 2014
Published: January 20, 2015

DOI: 10.1021/ic502637q
Inorg. Chem. 2015, 54, 1165−1177

In contrast, the seminal work of Kasuya and co-workers in 2004 characterized the *stoichiometric* (1:1) nanoclusters $(CdSe)_{13}$, $(CdSe)_{19}$, $(CdSe)_{33}$, and $(CdSe)_{34}$ by mass-spectrometric analysis of solution-derived synthetic mixtures.[11d] The structures and stabilities of the *stoichiometric* magic-size nanoclusters have been extensively studied theoretically;[16] however, to our knowledge, no X-ray crystal-structure determinations have been reported to date for any member of this stoichiometric family. The lack of structural data is largely due to the lack of syntheses that selectively produce nanoclusters of a single size. Most syntheses afford mixtures of the magic sizes,[10,11] which have not proven easily separable. Theoretical studies predict the stoichiometric, charge-neutral $(II-VI)_x$ nanoclusters to have cagelike structures, somewhat reminiscent of the carbon fullerenes.[16]

In 2012, we reported the first isolation of a single-size $(CdSe)_x$ nanocluster as the ligated derivative $[(CdSe)_{13}(n\text{-octylamine})_{13}]$.[11e] Additional $[(CdSe)_{13}(RNH_2)_{13}]$ derivatives with R = *n*-propyl, *n*-pentyl, and oleyl were subsequently obtained as slushy or normal solids on the gram scale.[11e,h] Shortly thereafter, Sardar and co-workers isolated a derivative of $(CdSe)_{34}$.[11f] We later described the synthesis of $[(CdSe)_{34}(n\text{-octylamine})_{16}(\text{di-}n\text{-pentylamine})_2]$.[11g]

Mechanistic studies established an unexpected formation pathway in our CdSe nanocluster syntheses (Scheme 1).[13a] The $(CdSe)_{13}$ nanoclusters were shown to grow within spontaneously formed, lamellar, primary-amine-bilayer templates (Scheme 1a,b). The nanoclusters were liberated from the templates by a ligand-exchange-driven unbundling process (Scheme 1c,d). Alternatively, mild heating (at 70−80 °C) of the template-assembled $(CdSe)_{13}$ nanoclusters resulted in their coalescence and recrystallization to afford wurtzitic CdSe quantum belts (ribbon-shaped nanocrystals; Scheme 1e). The flat morphology of the quantum belts was imposed by the lamellar structure of the template. We subsequently learned that flat wurtzitic CdSe quantum platelets (QPs) could be grown similarly from $(CdSe)_{34}$ at room temperature, a remarkably low growth temperature.[11g] We proposed that low-temperature growth was enabled because $(CdSe)_{34}$ is near the critical crystal-nucleus size for CdSe, and thus $[(CdSe)_{34}(n\text{-octylamine})_{16}(\text{di-}n\text{-pentylamine})_2]$ constitutes crystal nuclei that may be stored in a bottle. Thus, other magic-size nanoclusters like $(CdSe)_{13}$ and $(CdSe)_{34}$ are expected to be potent nanocrystal precursors.

Scheme 1. **Chemical Reaction Pathway for the Synthesis of II−VI Semiconductor Magic-Size Nanoclusters and Flat Colloidal Nanocrystals**[a]

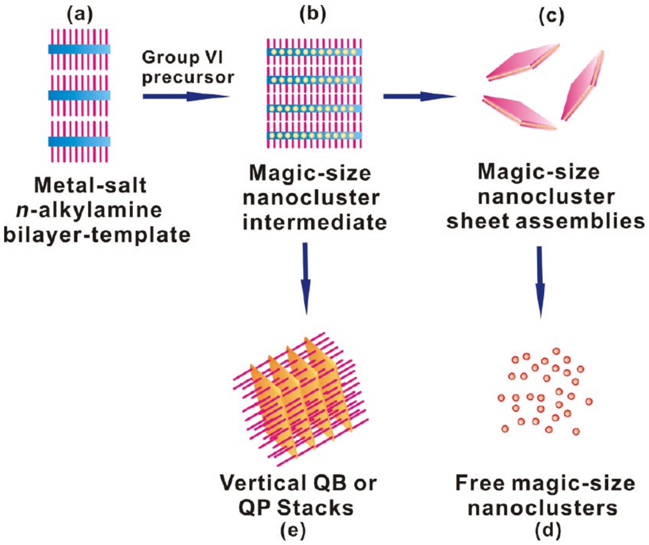

[a] (a) The combination of metal salts and the primary-amine solvents forms lamellar, primary-amine-bilayer templates. (b) The addition of group VI precursors results in the growth of magic-size nanoclusters within the templates. (c) Ligand exchange with oleylamine liberates sheetlike aggregates. (d) Further sonication breaks the templates and releases free magic-size nanoclusters. (e) Magic-size nanoclusters are converted to bundled QPs or belts under mild conditions.

The question addressed in this work is the extent to which the CdSe magic-size-nanocluster chemistry summarized above may be extended to other members of the II−VI family of semiconductors. We now report spectral data and other characterizations of primary-amine-ligated derivatives of $(CdS)_{34}$ and $(ZnS)_{34}$, which appear to be the most thermodynamically stable magic sizes for those compositions. This contrasts with our observations in the $(CdSe)_x$-nanocluster system, in which $(CdSe)_{13}$ was shown to be more stable than $(CdSe)_{34}$. Similarly, $(ZnSe)_{13}$, $(CdTe)_{13}$, and $(ZnTe)_{13}$, also isolated as primary-amine derivatives, appear to be the most stable magic sizes for those compositions. We also describe the conversion of several of these magic-size precursors into flat colloidal nanocrystals under mild conditions.

■ EXPERIMENTAL SECTION

Materials and General Procedures. Cadmium acetate dihydrate $[Cd(OAc)_2\cdot 2H_2O$, >98%], selenourea (98%), zinc acetate dihydrate $[Zn(OAc)_2\cdot 2H_2O$, >98%], zinc chloride (98%, ACS reagent), elemental tellurium power (Te, −5 to +50 mesh, 99.999%), tri-*n*-octylphosphine (TOP, 97%), Super-Hydride (lithium triethylborohydride, 1.0 M solution), thioacetamide (>99%), *n*-octylamine (+99%), and di-*n*-pentylamine (mixture of isomers, 99%) were obtained from Sigma-Aldrich. Sulfur powder (sublimed, >99%) was obtained from Strem Chemicals. All reagents were used as received and stored under N_2. Toluene (CHROMASOLV for HPLC, ≥99.9%), tetrahydrofuran (inhibitor-free, CHROMASOLV Plus, for HPLC, ≥99.9%), and cyclohexane (anhydrous, 99.5%) from Sigma-Aldrich were purged with dry N_2 for at least 3 h and stored under N_2 prior to use. Transmission electron microscopy (TEM) sample grids (Cu with holey C film) were obtained from Ted Pella, Inc.

All synthetic procedures were conducted under dry N_2, except the final washing steps, which were conducted in an ambient atmosphere for the CdS, ZnS, and ZnSe magic-size nanoclusters. The final washing steps were conducted under N_2 for the CdTe and ZnTe magic-size nanoclusters. The reaction mixtures were not stirred. The synthetic products were generally stored as reaction mixtures.

Analyses. Elemental analyses (C, H, and N) were obtained from Galbraith Laboratories, Inc. (Knoxville, TN). UV−visible spectra were obtained from a PerkinElmer Lambda 950 UV−visible spectrometer. IR spectra were obtained from a PerkinElmer Spectrum BX Fourier transform infrared system. The X-ray diffraction (XRD) patterns were obtained from a Rigaku Dmax A vertical powder diffractometer with Cu Kα radiation (λ = 1.5418 Å) and a Bruker d8 Advance X-ray diffractometer. Low-resolution TEM images were obtained from a JEOL 2000FX microscope operating at 200 kV.

Laser-desorption-ionization (LDI) mass spectra were obtained on an AB SCIEX Applied Biosystem Voyager DE-STR Workstation (Framingham, MA), using synthetic specimens as isolated, without a matrix. This instrument is incapable of isotopic-peak resolution, and thus the isotopomers of the $(II-VI)_x$ nanoclusters were unresolved. The resulting mass-distribution envelopes were fitted by modified Gaussian functions (*GaussMod* in *Origin* software), yielding the center of the envelopes as the mass centroid and the error in the central mass. These values are reported in the Results section.

Preparation of Tri-*n*-octylphosphine Telluride (TOPTe). A stock solution of TOPTe (1 M) in TOP was prepared by mixing Te powder (2.56 g, 20.0 mmol) in TOP (16.62 g, 20 mL) at room temperature, followed by heating of the mixture in an oil bath at 240 °C under N_2 for 0.5 h to form a light-yellow solution. When stored in a glovebox at room temperature, this stock solution remained stable and usable for at least 6 months.

Preparation of $[(CdS)_{34}(n\text{-butylamine})_{18}]$. In a typical procedure, $Cd(OAc)_2\cdot 2H_2O$ (44 mg, 0.17 mmol) was added to *n*-butylamine (3.8 g, 0.052 mol) in a septum-capped Schlenk tube, heated in a 60 °C oil bath for 1 h to achieve dissolution, and then allowed to cool to room temperature. In a glovebox, thioacetamide (6 mg, 0.080 mmol) was dissolved in *n*-butylamine (0.8 g, 0.011 mol) in a septum-capped amber vial and placed in a benchtop sonicator (5 min) to achieve dissolution.

The thioacetamide solution was injected into the cadmium-precursor solution at room temperature (20−25 °C) without stirring. The reaction mixture turned from clear to viscous in 3 h, and a white precipitate was formed at the bottom of the Schlenk tube overnight. The reaction mixture was subsequently heated at 60 °C in an oil bath for 40 min, during which time the precipitate remained white and the supernatant colorless.

The white precipitate was separated by centrifugation (1500 rpm, 5 min), and the colorless supernatant was discarded. The remaining white slush was redispersed in pure toluene (3−5 mL), and the mixture was recentrifuged and the supernatant discarded. This purification process was conducted at least five times in total, yielding $[(CdS)_{34}(n\text{-butylamine})_{18}]$ as a yellowish-white solid after drying in vacuo for 12 h (13.8 mg, 94%). IR (KBr, cm^{-1}, 25 °C): 3270 (w, NH stretch), 3200 (w, NH stretch), 3130 (w), 2958 (m), 2922 (vs), 2850 (vs), 1596 (s, NH_2 deformation), 1466 (s), 1378 (w), 1092 (w) 972 (w). UV−visible (toluene; λ_{max}, nm): 326, 361. Anal. Calcd for $[(CdS)_{34}(n\text{-butylamine})_{18}]$: C, 13.87; H, 3.20; N, 4.04. Found, C, 14.39; H, 3.20; N, 4.00. All values are given as percentages.

Other primary-amine derivatives of $(CdS)_{34}$ were synthesized under the same general conditions, except for the reaction solvent. *n*-Octylamine and *n*-propylamine were used respectively to form the white slushy solid $[(CdS)_{34}(n\text{-octylamine})_x]$ and the white solid $[(CdS)_{34}(n\text{-propylamine})_x]$.

Preparation of $[(ZnS)_{34}(n\text{-butylamine})_{34}]$. All synthetic procedures were conducted under the same general conditions as those used in the $[(CdS)_{34}(n\text{-butylamine})_{18}]$ synthesis, except for the zinc and sulfur precursors. $Zn(OAc)_2\cdot 2H_2O$ (45 mg, 0.20 mmol) was dissolved in *n*-butylamine (5.7 g, 0.078 mol), heated in a 70 °C oil bath for 1 h, and allowed to cool to room temperature. Sulfur powder (4 mg, 0.125 mmol) was combined with *n*-butylamine (1.2 g, 0.016 mol) in an amber vial and sonicated in a benchtop sonicator to achieve dissolution. The sulfur-precursor solution was injected into the $Zn(OAc)_2$ solution at room temperature without stirring. The color and consistency of the reaction mixture changed from colorless (0 min) to a viscous white (over 6 h) and to a cloudy white (over 10 h). After 1 day, a white precipitate formed under a colorless supernatant. The purification procedure was the same as that used in the synthesis of $[(CdS)_{34}(n\text{-butylamine})_{18}]$. The residual solvent was removed in vacuo, leaving $[(ZnS)_{34}(n\text{-butylamine})_{34}]$ as a white solid (20.6 mg, 97%). IR (KBr, cm^{-1}, 25 °C): 3226 (w, NH stretch), 3192 (sh, NH stretch), 3120 (m), 2956 (w), 2920 (s), 2872 (sh), 2848 (s), 1558 (s, NH_2 deformation), 1466 (w), 1066 (w), 980 (w). UV−visible (toluene; λ_{max}, nm): 258. Anal. Calcd for $[(ZnS)_{34}(n\text{-butylamine})_{18}]$: C, 28.13; H, 6.45; N, 8.20. Found, C, 28.83; H, 6.48; N, 7.75. All values are given as percentages.

The *n*-octylamine derivative of $(ZnS)_{34}$ was synthesized under the same general conditions, except for the reaction solvent. *n*-Octylamine was used to form $[(ZnS)_{34}(n\text{-octylamine})_x]$ as a gray slushy solid.

Preparation of $[(ZnSe)_{13}(n\text{-butylamine})_{13}]$. $Zn(OAc)_2\cdot 2H_2O$ (27 mg, 0.12 mmol) was dissolved in *n*-butylamine (2.9 g, 0.040 mol) in a septum-capped Schlenk tube, heated in a 70 °C oil bath for 1 h, and allowed to cool to room temperature. Selenourea (25 mg, 0.20 mmol) was combined with *n*-butylamine (0.6 g, 0.0082 mol) in the glovebox and then sonicated in a benchtop sonicator (5 min) to achieve dissolution.

The selenourea solution was injected into the $Zn(OAc)_2$ solution at room temperature (20−25 °C) without stirring. The color of the reaction mixture changed immediately after injection from colorless (0 min) to clear light orange (5 s), viscous light orange (15 s), and orange with a white suspension (cloudy, 15 min). After 3 h without stirring, $(ZnSe)_{13}$ was deposited as an orange-white precipitate under an orange-red supernatant. The reaction mixture was subsequently heated at 70 °C in an oil bath for 40 min, during which the mixture turned a darker shade of orange red, with a white precipitate. TOP (65 mg) was injected to convert the selenium side products to soluble TOPSe, resulting in a colorless solution with a white precipitate.

The purification procedure was the same as that used in the synthesis of $[(CdS)_{34}(n\text{-butylamine})_{18}]$. The residual solvent was removed in vacuo, leaving $[(ZnSe)_{13}(n\text{-butylamine})_{13}]$ as a white solid (24.4 mg, 91.2%). IR (KBr, cm^{-1}, 25 °C): 3234 (w, NH stretch), 3196 (sh, NH stretch), 3118 (m), 2956 (w), 2920 (s), 2860 (sh), 2848 (s), 1594 (s, NH_2 deformation), 1468 (w), 1352 (w), 1066 (w), 978 (w). UV−visible (toluene; λ_{max}, nm): 279, 289. Anal. Calcd for $[(ZnSe)_{13}(n\text{-butylamine})_{13}]$: C, 22.07; H, 5.06; N, 6.44. Found, C, 22.79; H, 5.30; N, 6.82. All values are given as percentages.

The *n*-octylamine derivative of $(ZnSe)_{13}$ was synthesized under the same general conditions, except for the reaction solvent. *n*-Octylamine was used to form $[(ZnSe)_{13}(n\text{-octylamine})_x]$ as a white slushy solid.

Preparation of $[(CdTe)_{13}(n\text{-propylamine})_{13}]$. In a typical synthesis, a solution of the cadmium precursor was prepared by dissolving $Cd(OAc)_2\cdot 2H_2O$ (33 mg, 0.12 mmol) in *n*-propylamine (2.9 g, 0.049 mol) in a septum-capped Schlenk tube. The mixture was heated in a 50 °C oil bath under N_2 for over 1 h and then allowed to cool to room temperature. In a glovebox, TOPTe (0.125 g, 1 M) and Super-Hydride (0.125 g, 1 M) were combined in a separate amber vial to generate a light-purple milky suspension, and then *n*-propylamine (0.5 g, 8.46 mmol) was added to form a dark-purple tellurium-precursor solution.

The tellurium-precursor solution was injected into the cadmium-precursor solution at room temperature (20−25 °C) without stirring. The reaction mixture turned from colorless to pale yellow (clear) immediately after injection, to a viscous yellow in 30 s, to a yellowish green in 2 min, and to a milky yellowish white after 15 min. A white precipitate was formed at the bottom of the Schlenk tube in 2 h after injection, under a clear light-yellow supernatant. The reaction mixture was subsequently heated at 50 °C in an oil bath for 40 min, during which the precipitate remained white and the supernatant became colorless.

The white precipitate was purified with dry toluene using at least three centrifugation cycles as described above for the $[(CdS)_{34}(n\text{-butylamine})_{18}]$ synthesis, with these steps were conducted under dry N_2. This workup yielded $[(CdTe)_{13}(n\text{-propylamine})_{13}]$ as a gray solid after drying in vacuo for 12 h (35.0 mg, 94%). IR (KBr, cm^{-1}, 25 °C): 3270 (w, NH stretch), 3216 (w, NH stretch), 3128 (w), 2956 (m), 2850 (vs), 1574 (s, NH_2 deformation), 1424 (s), 1348 (w), 1018 (w). UV−visible (toluene; λ_{max}, nm): 354, 375. Anal. Calcd for $[(CdTe)_{13}(n\text{-propylamine})_{13}]$: C, 12.04; H, 3.00; N, 4.60. Found, C, 12.01; H, 3.02; N, 4.40. All values are given as percentages.

The *n*-octylamine derivative of $(CdTe)_{13}$ was synthesized under the same general conditions, except for the reaction solvent. *n*-Octylamine was used to form $[(CdTe)_{13}(n\text{-octylamine})_x]$ as a gray slushy solid.

Preparation of $[(ZnTe)_{13}(n\text{-butylamine})_{13}]$. The synthesis was conducted under the same general conditions as those used in the $[(CdTe)_{13}(n\text{-propylamine})_{13}]$ synthesis, except for the zinc precursor. $Zn(OAc)_2\cdot 2H_2O$ (27 mg, 0.12 mmol) was dissolved in *n*-butylamine (2.9 g, 0.040 mol), heated in a 70 °C oil bath for 1 h, and transferred to a 50 °C oil bath. In a glovebox, a TOPTe stock solution (0.125 g, 1 M) and a Super-Hydride solution (0.125 g, 1 M) were combined in a separate amber vial to generate a light-purple milky dispersion, and then *n*-butylamine (0.5 g, 0.0068 mol) was added to form a dark-red tellurium-precursor solution.

The tellurium-precursor solution was injected into the zinc-precursor solution held at 50 °C. The resulting mixture became viscous and white within a few seconds after injection, a milky white after 5 min, and a white precipitate under a clear, colorless supernatant after 30 min. The reaction mixture was subsequently heated at 70 °C in an oil bath for 40 min, during which the precipitate remained white and the supernatant colorless.

The purification procedure was the same as that used in the synthesis of $[(CdTe)_{13}(n\text{-butylamine})_{13}]$, with each of the steps conducted under dry N_2. The residual solvent was removed in vacuo, leaving $[(ZnTe)_{13}(n\text{-butylamine})_{13}]$ as a white solid (31.0 mg, 95%). IR (KBr, cm^{-1}, 25 °C): 3234 (w, NH stretch), 3190 (sh, NH stretch), 3118 (m), 3128 (m), 2956 (w), 2920 (s), 2850 (s), 1576 (s, NH_2 deformation), 1466 (w), 1036 (w), 970 (w). UV−visible (toluene; λ_{max}, nm): 302, 323. Anal. Calcd for $[(ZnTe)_{13}(n\text{-butylamine})_{13}]$: C, 18.04; H, 4.13; N, 5.20. Found, C, 18.27; H, 3.95; N, 5.27. All values are given as percentages.

The *n*-octylamine derivative of $(ZnTe)_{13}$ was synthesized under the same general conditions, except for the reaction solvent. *n*-Octylamine was used to form $[(ZnTe)_{13}(n\text{-octylamine})_x]$ as a white slushy solid.

Preparation of CdS QPs. In a typical synthesis, $Cd(OAc)_2{\cdot}2H_2O$ (54 mg, 0.20 mmol) was combined with di-*n*-pentylamine (5.7 g, 24 mmol) in a septum-capped Schlenk tube, placed in a benchtop sonicator to achieve dissolution, and then stored in an ice bath (0 °C) inside a refrigerator. In a glovebox, thioacetamide (30 mg, 0.40 mmol) was combined with *n*-octylamine (1.8 g, 14 mmol) in a septum-capped amber vial. The vial was removed from the glovebox and placed in a benchtop sonicator bath (10 min) to achieve dissolution.

The thioacetamide solution was injected into the cadmium-precursor solution held at 0 °C. The colorless reaction mixture turned a cloudy light green in 10 s, and a yellowish-white precipitate began to form after 2 h. After 1 day, the yellowish-white precipitate remained in the presence of a colorless supernatant. The precipitate consisted of bundled CdS QPs, which were stored in the reaction mixture at 0 °C under N_2 for subsequent analyses.

Preparation of ZnS QPs. In a typical synthesis, $Zn(OAc)_2{\cdot}2H_2O$ (56 mg, 0.26 mmol) was dissolved in octylamine (5.74 g, 44 mmol) in a septum-capped Schlenk tube and the mixture was heated at 70 °C for 1 h to achieve dissolution. In a glovebox, thioacetamide (30 mg, 0.40 mmol) was dissolved in *n*-octylamine (1.2 g, 9.3 mmol) in a septum-capped amber vial.

The thioacetamide solution was injected into the zinc-precursor solution at 100 °C without stirring. The color of the reaction mixture immediately changed from colorless to a cloudy white. The reaction mixture remained at 100 °C for 22 h, during which the ZnS QPs were deposited as a white precipitate under a cloudy white supernatant. The ZnS QPs were then stored at room temperature in the reaction mixture under N_2 for further analyses.

Preparation of ZnSe QPs. In a typical synthesis, $Zn(OAc)_2{\cdot}2H_2O$ (56 mg, 0.26 mmol) was combined with di-*n*-octylamine (5.74 g, 24 mmol) at room temperature in a septum-capped Schlenk tube and placed in a benchtop sonicator (5 min) to achieve dissolution. (We note that $Zn(OAc)_2{\cdot}2H_2O$ hydrolyzes to ZnO in long-chain secondary-amine solvents at temperatures above ca. 70 °C.) In a glovebox, selenourea (50 mg, 0.41 mmol) was combined with *n*-octylamine (1.2 g, 9.3 mmol) in a septum-capped amber vial and then transferred to a benchtop sonicator (5 min) to achieve dissolution.

The selenourea solution was injected into the zinc-precursor solution held at 100 °C in an oil bath without stirring. The color of the reaction mixture changed from colorless to a light orange (5 s), a viscous light orange (1 min), and a cloudy orange with a white precipitate (5 min). After the reaction mixture stood for overnight at 100 °C without stirring, the ZnSe QPs were deposited as a white precipitate under a red supernatant containing the selenium side products. TOP (65 mg) was injected to convert the selenium side products to soluble TOPSe, resulting in a colorless solution with a white precipitate. The white precipitate of bundled ZnSe QPs was then stored at room temperature in the reaction mixture under N_2 for further analyses.

Preparation of CdTe QPs. In a typical synthesis, $Cd(OAc)_2{\cdot}2H_2O$ (33 mg, 0.12 mmol) was dissolved in di-*n*-pentylamine (2.8 g, 18 mmol) in a septum-capped Schlenk tube, placed in a benchtop sonicator bath to achieve dissolution, and then transferred to 70 °C in an oil bath. In a glovebox, TOPTe (0.125 g, 1 M) and Super-Hydride (0.05 g, 1 M) were combined in a separate amber vial to generate a light-purple milky dispersion, and then *n*-octylamine (0.6 g, 0.0046 mol) was added to form a dark-purple tellurium-precursor solution.

The tellurium precursor was injected into the cadmium-precursor solution at 70 °C without stirring. The colorless reaction mixture turned to light yellow immediately, viscous yellow in 5 s, cloudy and yellowish within 30 min, and cloudy and white in 8 h. After 1 day, CdTe QPs were deposited as a white precipitate under a colorless supernatant. The white precipitate consisted of bundled CdTe QPs, which were stored in the reaction mixture at room temperature under N_2 for subsequent analyses.

■ RESULTS

Zinc(II)-Containing Amine-Bilayer Mesophases. Hyeon and co-workers first reported that the dissolution of $CdCl_2$ in primary-amine solvents resulted in the formation of lamellar, amine-bilayer mesophases (Scheme 1a), which templated the growth of flat, colloidal CdSe nanosheets.[17] We subsequently demonstrated that analogous mesophase templates were prepared using CdI_2 and $Cd(OAc)_2{\cdot}2H_2O$.[13a] Moreover, we found that these templates provided ideal environments for the preparation of amine-ligated derivatives of the single-size nanoclusters $(CdSe)_{13}$ and $(CdSe)_{34}$. Because a goal of the present work was to prepare magic-size nanoclusters of ZnS, ZnSe, and ZnTe, we sought to determine if lamellar, amine-bilayer mesophases formed with zinc salts.

The zinc compounds $ZnCl_2$ and $Zn(OAc)_2{\cdot}2H_2O$ were separately added to primary-amine solvents and heated to 70 °C. After the respective solutions were cooled to room temperature, they were combined with hexane, resulting in the precipitation of white or slushy solids. Low-angle XRD patterns of the precipitates are given in Figure 1. These patterns evidence the formation of lamellar, amine-bilayer mesophases (Scheme 1a) analogous to those formed from cadmium salts. The lamellar *d* spacings extracted from the XRD data are plotted versus the number of carbon atoms in the primary-amine alkyl chain (Figure S1 in the Supporting Information, SI). These plots were linear as expected.[18] The *y* intercepts of the plots measured the distance between the amine head groups in the amine bilayers and were 0.55 and 0.51 nm for the $ZnCl_2$ and $Zn(OAc)_2{\cdot}2H_2O$ mesophases, respectively. The results established that the zinc precursors spontaneously formed lamellar, amine-bilayer template structures, as previously found for the cadmium precursors.

$(CdS)_{34}$ and $(ZnS)_{34}$ Derivatives. Primary-amine derivatives of $(CdS)_{34}$ and $(ZnS)_{34}$ were prepared by reaction of the corresponding $Cd(OAc)_2{\cdot}2H_2O$ and $Zn(OAc)_2{\cdot}2H_2O$ amine-bilayer mesophases with thioacetamide and sulfur, respectively, at room temperature. The absorption spectrum of the *n*-octylamine derivative of $(CdS)_{34}$ (Figure 2a) contained sharp features at 361 and 326 nm and was nominally similar to those exhibited by amine derivatives of $(CdSe)_{34}$ (Figure S2b,c in the SI), except blue-shifted as expected by about 60 nm. (The λ_{max} values in the absorption spectra of the nanoclusters discussed here are listed in Table 1.) We note that the spectrum of $(CdS)_{34}$ was red-shifted relative to that of $[(CdSe)_{13}(n\text{-octylamine})_{13}]$, confirming that it must be larger than $(CdS)_{13}$. If the nanocluster we assigned as $(CdS)_{34}$ was actually

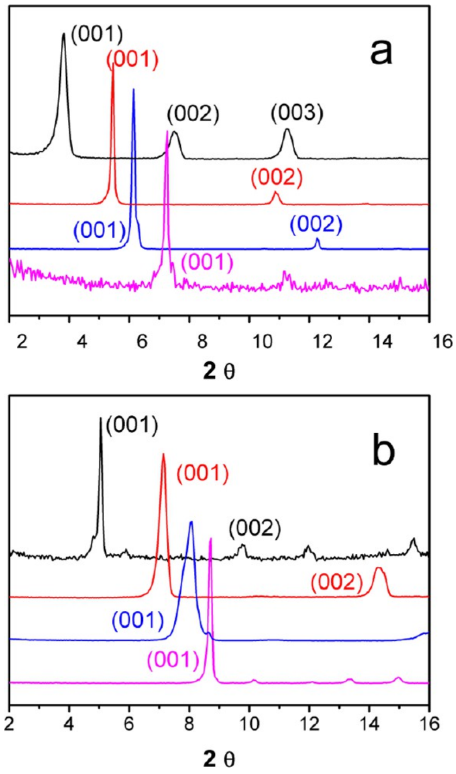

Figure 1. Low-angle XRD patterns of the zinc precursors (a) $[ZnCl_2(L)_2]$ and (b) $[Zn(OAc)_2(L)_2]$ showing the basal reflections produced by the lamellar mesostructures. From top to bottom, L = *n*-octylamine (black), *n*-pentylamine (red), *n*-butylamine (blue), and *n*-propylamine (magenta).

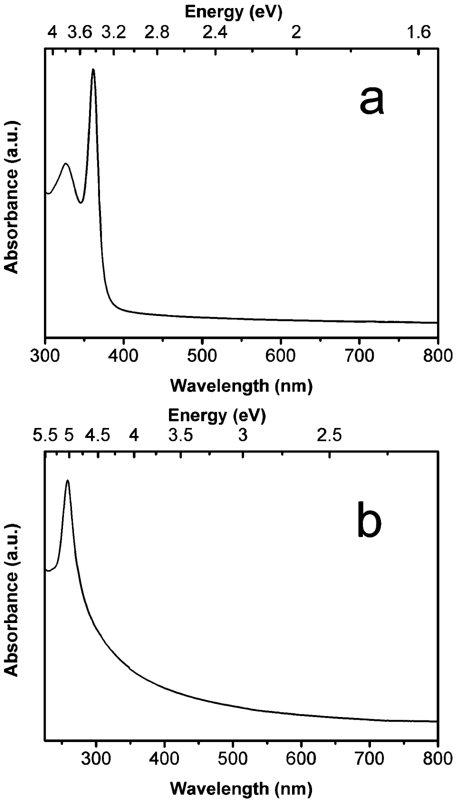

Figure 2. UV–visible absorption spectra (in toluene dispersion) of (a) $[(CdS)_{34}(n\text{-octylamine})_x]$ and (b) $[(ZnS)_{34}(n\text{-butylamine})_{34}]$.

Table 1. Λ_{max} Values in the Absorption Spectra of the II–VI Nanoclusters, QPs, and Quantum Belts

	λ_{max} (nm)		
nanoclusters/QPs	first absorption	second absorption	third absorption
$(CdS)_{34}(n\text{-butylamine})_{18}$	361	326	
$(CdSe)_{34}(n\text{-octylamine})_{16}(\text{di-}n\text{-pentylamine})_{13}$[11g]	418	390	355
$(ZnS)_{34}(n\text{-butylamine})_{34}$	258		
$(CdSe)_{13}(n\text{-octylamine})_{13}$[11e]	350	332	315
$(ZnSe)_{13}$ $(n\text{-butylamine})_{13}$	289	279	
$(CdTe)_{13}(n\text{-octylamine})_{13}$	373	353	
$(ZnTe)_{13}(n\text{-butylamine})_{13}$	323	302	
CdS QPs	375	337	
ZnS QPs	282		
CdSe QPs[11g]	448	423	375
ZnSe QPs	347	329	304
CdTe quantum belts	491	444	

$(CdS)_{13}$, then its spectrum would be blue-shifted relative to that of $[(CdSe)_{13}(n\text{-octylamine})_{13}]$.

The absorption spectrum of the *n*-butylamine derivative of $(ZnS)_{34}$ (Figure 2b) contained a single sharp feature at 258 nm, blue-shifted by about 100 nm from the spectrum of $(CdS)_{34}$ (Figure 2a and Table 1). Presumably, its higher energy features were obscured by solvent absorptions. The spectra of additional amine derivatives of $(CdS)_{34}$ and $(ZnS)_{34}$ (Figure S3 in the SI) corresponded closely to those in Figure 2. Whereas $(CdSe)_{34}$ was previously found to be a kinetic product that converted to $(CdSe)_{13}$ under the general conditions employed here,[11g,13a] no similar transformations of $(CdS)_{34}$ and $(ZnS)_{34}$ were observed. The absorption spectra of amine derivatives of $(CdS)_{34}$ and $(ZnS)_{34}$ were unchanged after several days at room temperature.

The LDI mass spectra of $(CdS)_{34}$ and $(ZnS)_{34}$ derivatives are given in Figure 3. These contained prominent peaks corresponding to the bare nanoclusters $(CdS)_{34}$ and $(ZnS)_{34}$ at m/z 4912 ± 9 and 3310 ± 9, respectively, as well as a sequence of fragment ions, including those corresponding to $(CdS)_{33}$, $(CdS)_{13}$, $(ZnS)_{33}$, and $(ZnS)_{13}$. As in the derivatives of $(CdSe)_{13}$ and $(CdS)_{34}$,[11d,e] LDI resulted in dissociation of the amine ligands prior to mass-spectral analysis.

Elemental analyses of isolated derivatives indicated the formulas $[(CdS)_{34}(n\text{-butylamine})_{18}]$ and $[(ZnS)_{34}(n\text{-butylamine})_{34}]$. The number of amine ligands in the $(CdS)_{34}$ derivative equaled the number previously found in $[(CdSe)_{34}(n\text{-octylamine})_{16}(\text{di-}n\text{-pentylamine})_2]$,[11g] whereas the 1:1 ligand-to-Zn ratio in $[(ZnS)_{34}(n\text{-butylamine})_{34}]$ corresponded to the similar 1:1 ratios found in the $[(CdSe)_{13}(\text{primary amine})_{13}]$ derivatives. Both isolated derivatives were obtained as solids in high yields.[11e,h]

TEM images (Figures 4 and S4b in the SI) of the *n*-octylamine derivative of $(ZnS)_{34}$ exhibited clear parallel-fringe patterns indicative of the bundled, template structure entraining the nanoclusters (Scheme 1b). Fringe patterns in the corresponding images of the *n*-propylamine derivative of $(CdS)_{34}$ were not evident, but the wispy morphologies observed were consistent with those previously obtained of the bundled, templated assemblies of $[(CdSe)_{13}(n\text{-octylamine})_{13}]$ (Figure S4a in the SI).[13a]

$(ZnSe)_{13}$, $(CdTe)_{13}$, and $(ZnTe)_{13}$ Derivatives. Primary-amine derivatives of $(ZnSe)_{13}$ were prepared by the reaction of

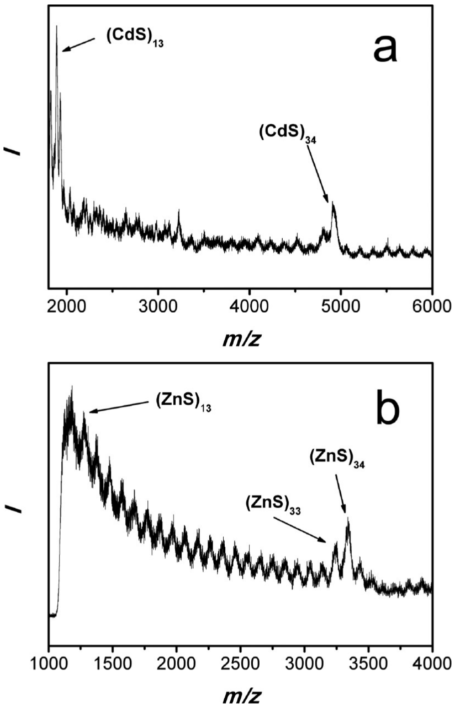

Figure 3. LDI mass spectra of (a) [$(CdS)_{34}$(n-butylamine)$_{18}$] and (b) [$(ZnS)_{34}$(n-butylamine)$_{34}$]. The peaks for the magic-size CdS nanoclusters are labeled.

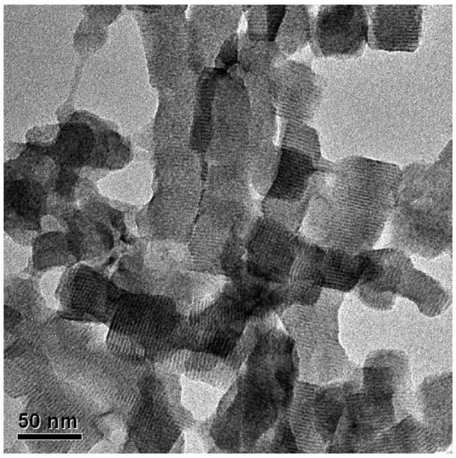

Figure 4. TEM image of the as-made bundled n-octylamine derivative of $(ZnS)_{34}$.

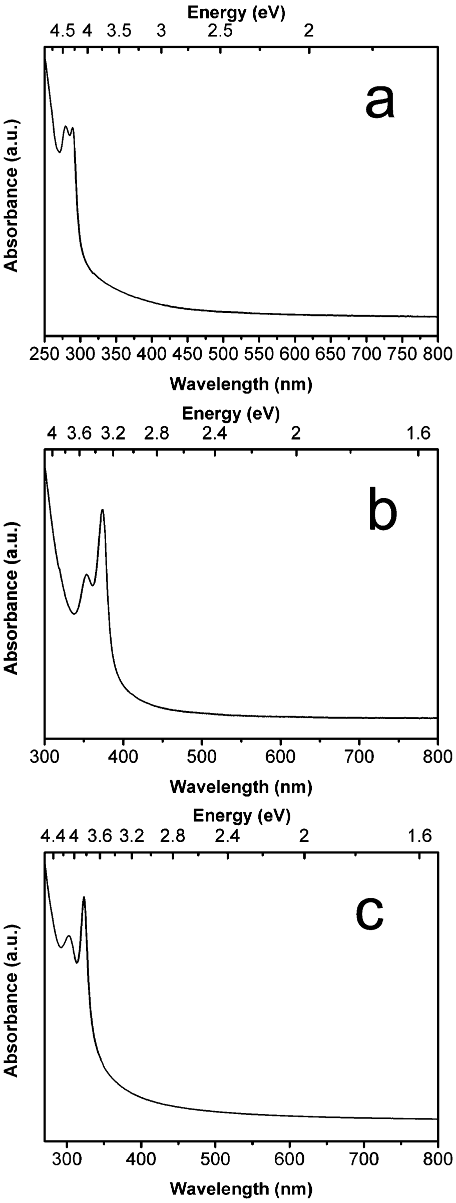

Figure 5. UV–visible absorption spectra (in toluene dispersion) of unbundled (a) [$(ZnSe)_{13}$(n-butylamine)$_{13}$], (b) [$(CdTe)_{13}$(n-octylamine)$_x$], and (c) [$(ZnTe)_{13}$(n-octylamine)$_x$].

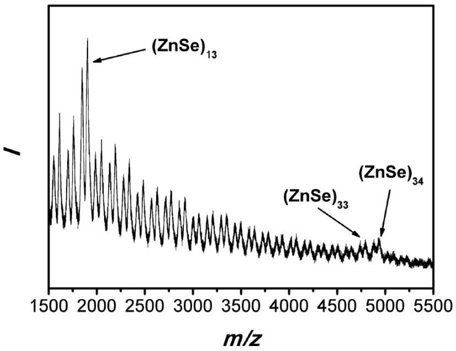

Figure 6. LDI mass spectrum of [$(ZnSe)_{13}$(n-octylamine)$_x$]. The peaks for the magic-size ZnSe nanoclusters are labeled.

$Zn(OAc)_2 \cdot 2H_2O$ amine-bilayer mesophases with selenourea at room temperature. The absorption spectrum of the n-butylamine derivative (Figures 5a and S5a in the SI) contained a sharp doublet-like feature of two closely spaced absorptions at 279 and 289 nm (Table 1). The spectrum closely resembled the corresponding doublet-like spectral feature of amine-ligated $(CdSe)_{13}$ (Figure S2a in the SI), except blue-shifted as expected by about 60 nm. This derivative was isolated as a white solid in high yield having an elemental analysis corresponding to that of [$(ZnSe)_{13}$(n-butylamine)$_{13}$]. The ligand-to-metal ratio of 1:1 was identical with those previously determined for the primary-amine derivatives of $(CdSe)_{13}$.[11e,h]

The LDI mass spectrum of the n-octylamine derivative of $(ZnSe)_{13}$ is given in Figure 6, in which $(ZnSe)_{13}$ is the base peak. However, a continuous series of other $(ZnSe)_x$ nanocluster ions extending upward to $(ZnSe)_{34}$ was observed. As in the case of [$(CdSe)_{13}$(n-octylamine)$_{13}$],[11e] we argue that the larger nanoclusters were generated by thermal excitation during laser desorption, during which the stabilizing ligands are dissociated. The absorption spectrum of $[(ZnSe)_{13}(n\text{-butylamine})_{13}]$ (Figure 5a) would not be as sharp and clean as observed if these larger sizes were truly present in the isolated derivative. Even so, the mass-spectral data do not provide evidence that $(ZnSe)_{13}$ was isolated in a single size; the absorption data provide stronger evidence of that.

TEM images of the bundled, template structures of the *n*-propylamine derivative of $(ZnSe)_{13}$ are given in Figure 7a,b. The bundles entraining the nanoclusters had a pseudorectangular morphology. The striations evident in Figure 7b may be indicative of the semicrystalline ordering of $(ZnSe)_{13}$ within template layers, as we found for $[(CdSe)_{13}(n\text{-octylamine})_{13}]$.[11h]

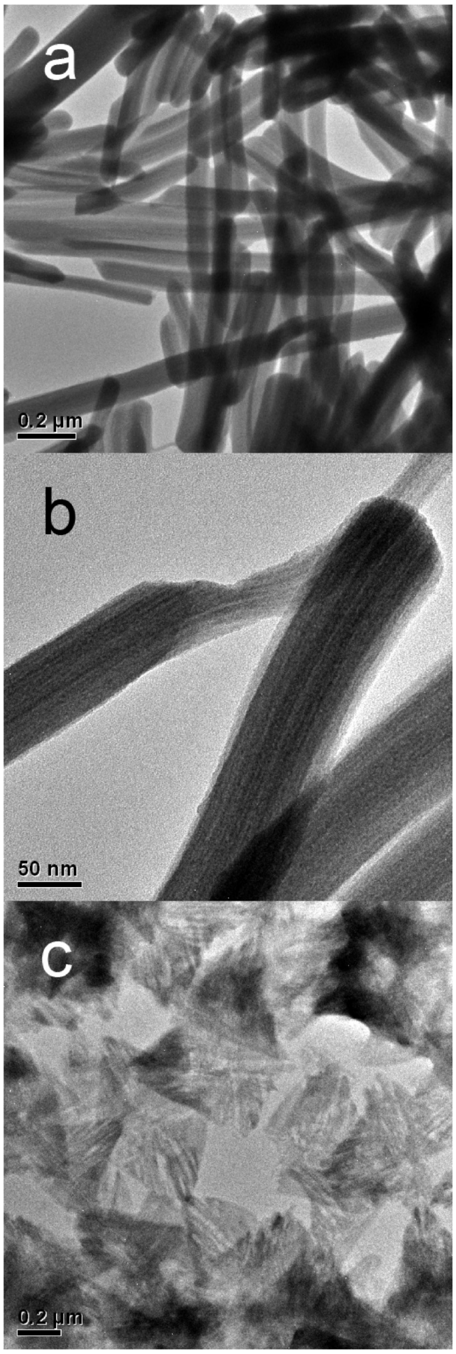

Figure 7. TEM images (a and b) of the bundled, template structures of the *n*-propyl amine derivative of $(ZnSe)_{13}$ and (c) exfoliated sheets of the *n*-octylamine derivative of $(CdTe)_{13}$.

Primary-amine derivatives of $(CdTe)_{13}$ and $(ZnTe)_{13}$ were prepared by reaction of the corresponding $Cd(OAc)_2{\cdot}2H_2O$ and $Zn(OAc)_2{\cdot}2H_2O$ amine-bilayer mesophases with TOPTe in the presence of Super-Hydride[19] at room temperature and 50 °C, respectively. The absorption spectra of the *n*-octylamine derivatives (Figures 5b and S5c in the SI and Figures 5c and S5e in the SI) contained asymmetric doublet features comparable to those of $(CdSe)_{13}$ and $(ZnSe)_{13}$ (Figures S2a in the SI and 5a). The separations of the peak maxima for the doublet features in the telluride nanoclusters (about 20 nm) were nearly the same as that in $(CdSe)_{13}$ (18 nm) and twice that in $(ZnSe)_{13}$ (10 nm). The observation of these doublet features in the tellurides was consistent with their assignment as $(II{-}VI)_{13}$ nanoclusters, as were the positions (λ_{max} values) of their absorptions, as analyzed below.

The doublet maxima in $(CdTe)_{13}$ (373 and 353 nm; Figure 5b and Table 1) were red-shifted from those of $(CdSe)_{13}$ (350 and 332 nm; Figure S2a in the SI) and blue-shifted relative to the absorptions of $(CdSe)_{34}$ (418, 390, and 355 nm; Figure S2b,c in the SI). If $(CdTe)_{13}$ were actually $(CdTe)_{34}$, its absorptions would have been red-shifted relative to those of $(CdSe)_{34}$. The doublet maxima in $(ZnTe)_{13}$ (323 and 302 nm; Figure 5c) were red-shifted from those of $(ZnSe)_{13}$ (289 and 279 nm; Figure 5a), as expected. Thus, the comparative absorption data for the telluride nanoclusters were fully consistent with their assignment as amine derivatives of $(CdTe)_{13}$ and $(ZnTe)_{13}$.

The telluride nanoclusters were isolated in high yields as the white-gray and white solids $[(CdTe)_{13}(n\text{-propylamine})_{13}]$ and $[(ZnTe)_{13}(n\text{-butylamine})_{13}]$, respectively. As in the primary-amine derivatives of $(CdSe)_{13}$ and $(ZnSe)_{13}$, the ligand-to-metal ratio was 1:1 in these isolated telluride derivatives. Solutions of ligated $(ZnTe)_{13}$ and the isolated derivative blackened within 5 min upon exposure to air. Solutions of ligated $(CdTe)_{13}$ and the isolated derivative were somewhat more air-stable and blackened within 1 day upon exposure. Unfortunately, both were too unstable to the atmosphere and under laser irradiation for LDI mass-spectral characterization.

Because of its instability, we were unable to obtain TEM images of ligated $(ZnTe)_{13}$. A TEM image of the *n*-octylamine derivative of $(CdTe)_{13}$ is given in Figure 7c. The triangular morphologies observed closely resembled the analogous sheets exfoliated from the templated bundles of $[(CdSe)_{13}(\text{primary amine})_{13}]$.[11h] The strip patterns evident in the $(CdTe)_{13}$-containing sheets may be due to the semicrystalline ordering of the nanoclusters. However, the sheets were unstable under the electron beam in the TEM, and some of the white features were holes in the sheets that developed during imaging.

Formation of II–VI QPs. In previous studies, we showed that nanocluster syntheses conducted in primary-amine solvents at room temperature produced $[(CdSe)_{13}(\text{primary amine})_{13}]$ nanoclusters,[11e,h] whereas those conducted in primary-amine–secondary-amine cosolvent mixtures under the same conditions afforded larger $(CdSe)_{34}$ nanoclusters, which were isolated as the derivative $[(CdSe)_{34}(n\text{-octylamine})_{16}(\text{di-}n\text{-pentylamine})_2]$.[11g] When the cosolvent reaction mixtures in which $(CdSe)_{34}$ was synthesized were held at room temperature, the nanoclusters coalesced to afford *crystalline* CdSe QPs. Alternatively, when identical reaction mixtures were held at 0 °C, $(CdSe)_{34}$ was converted to $(CdSe)_{13}$, showing it to be thermodynamically unstable with respect to the smaller nanocluster under the conditions employed. The results established the magic-size CdSe nanoclusters to be useful nanocrystal precursors, with $(CdSe)_{34}$ being remarkably effective, even at room temperature. In this work, we sought to determine if other magic-size II–VI nanoclusters would be similarly effective nanocrystal precursors.

CdS QPs. As in the CdSe example above, we conducted the CdS nanocluster synthesis in an *n*-octylamine–di-*n*-pentylamine cosolvent mixture, in this case at 0 °C. Reaction monitoring by absorption spectroscopy established the intermediacy of the $(CdS)_{34}$ nanoclusters (Figure S6 in the SI), as characterized above. After 1 day at 0 °C, the absorptions for $(CdS)_{34}$ were replaced by those of CdS QPs (Figure 8a).

The absorption spectrum matched those previously reported for CdS QPs synthesized at higher temperatures and having a thickness of 1.5 nm.[20] Two prominent absorptions were observed at 375 and 337 nm, assigned to the 1_h–1_e and 2_h–2_e quantum-well transitions in the platelets, respectively.[21] The platelets were found to have the wurtzite structure (see below), and a light-hole–heavy-hole splitting does exist in wurtzitic CdS. However, the light- and heavy-hole effective masses are very similar,[22] and the splitting was not resolved in the 1_h–1_e and 2_h–2_e features (Figure 8a) at the small thickness of these QPs.[23] Observation of the quantum-well spectrum established quantum confinement to be primarily in one dimension, the thickness dimension, and to be relaxed in the lateral dimensions, as previously observed for other CdS QPs.[20,23]

The XRD pattern (Figure 9a) of the as-synthesized CdS QPs was broadened by the thin dimension of the nanocrystals but clearly indexed to the wurtzite structure. The lattice parameters a = 3.98 Å and c = 6.63 Å were contracted relative to the bulk values by 3.7% and 1.8%, respectively (Table 2). Such lattice contractions are common in flat, colloidal, semiconductor nanocrystals having amine ligation and wurtzite structures.[21] In contrast, flat, colloidal, semiconductor nanocrystals having carboxylate ligation and zinc blende structures generally exhibit lattice dilations (expansions). Peng and co-workers measured dilations in the range of 0–4% in zinc blende CdS quantum disks.[20a] These lattice contractions and dilations are attributed to surface reconstructions, which may have either a compressive or tensile character.[21]

A TEM image of the CdS QPs is given in Figure 10a. The image contains unbundled platelets of rectangular morphology displaying their broad top (bottom) surfaces. The mean length (30–40 nm) and mean width (~5 nm) are smaller in comparison to other flat, colloidal CdS nanocrystals[20,23] and likely a result of the low synthesis temperature employed here. The thickness dimension is not discernible in the TEM images and is best estimated at 1.5 nm from the absorption data (see above).

ZnS QPs. Attempts to prepare ZnS QPs in primary-amine and secondary-amine cosolvents gave ambiguous results. Therefore, the synthesis was conducted in *n*-octylamine at 100 °C. Reaction monitoring by absorption spectroscopy established the intermediacy of $(ZnS)_{34}$ nanoclusters (Figure S7 in the SI), as characterized above.

The absorption spectrum of ZnS QPs, given in Figure 8b, contained one sharp feature at 282 nm, red-shifted by 24 nm from the absorption feature of the $(ZnS)_{34}$ precursor (Table 1). We assign the 282 nm absorption feature to the 1_h–1_e quantum-well transition. The platelets have the wurtzite structure (see below), and light-hole–heavy-hole splitting does not exist in wurtzitic ZnS. The higher-energy 2_h–2_e feature was presumably obscured by solvent absorption.

Two earlier studies of ZnS nanosheets found absorption features at 350[24] and 306 nm,[25] respectively. The thicknesses of

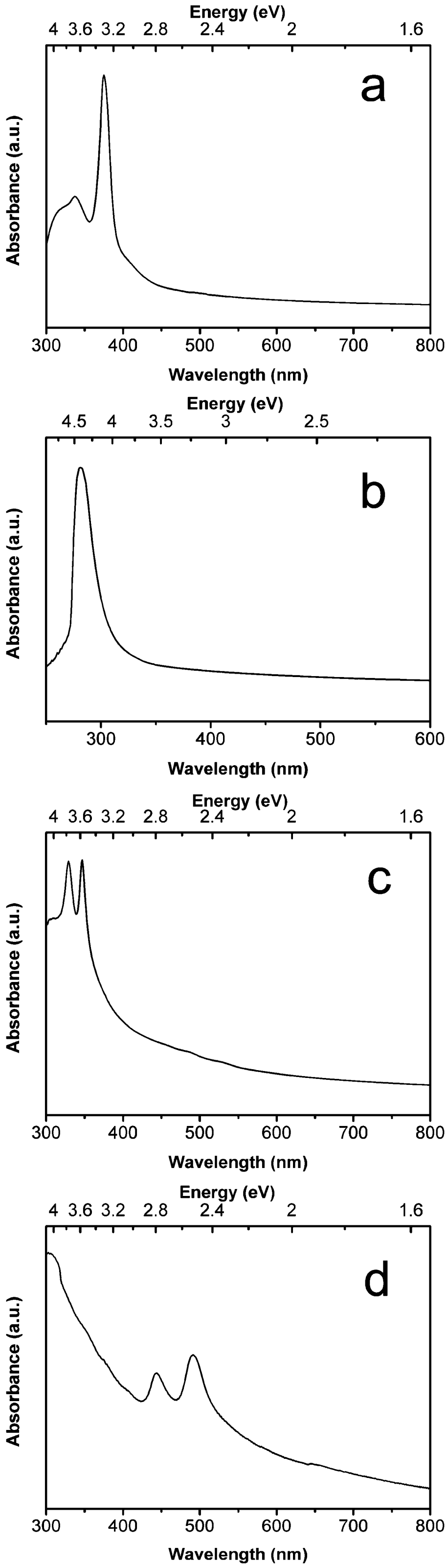

Figure 8. UV–visible absorption spectra (in toluene dispersion) of as-made bundled (a) CdS QPs, (b) ZnS QPs, (c) ZnSe QPs, and (d) CdTe quantum belts.

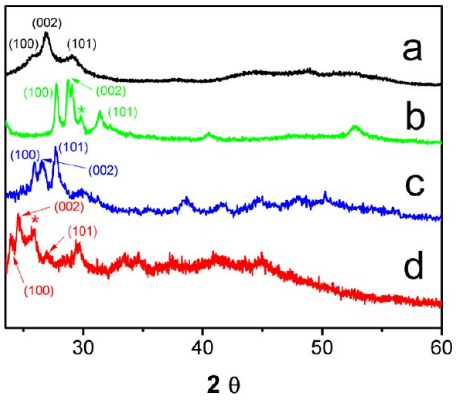

Figure 9. XRD patterns of (a) CdS QPs, (b) ZnS QPs, (c) ZnSe QPs, and (d) CdTe quantum belts. The indexed reflections are shifted to higher angle than that in the bulk patterns by lattice contractions (see the text). The asterisks identify unassigned peaks.

Table 2. Contraction of Lattice Parameters in Wurtzite QPs and Quantum Belts

	percent contraction (%)	
quantum nanocrystals	*a*	*c*
CdS QPs	3.7	1.8
ZnS QPs	2.7	0.2
CdSe QPs[11g]	5.4	2.9
ZnSe QPs	2.5	1.3
CdTe quantum belts	6.5	2.7

the nanosheets was not determined, but presumably they were thicker than those prepared here. More recently, ZnS-nanosheet syntheses have resulted in specimens having absorption features at 266–267 nm.[26] Because these features are slightly blue-shifted from our observation, they may be thinner nanosheets than those reported here. However, the ZnS nanosheet thicknesses have not yet been determined, including by us, so correlation of the spectral data to nanosheet thickness requires further work.

The XRD pattern of the ZnS QPs (Figure 9b) was sharp, likely because of the higher synthesis temperature employed, and indexed to the wurtzite structure. A few extraneous reflections were observed (identified in Figure 9b), as is common for QP specimens (see ref 11g and the Supporting Information in ref 27). A reflection at $2\theta = 29.08°$ appeared to be consistent in sharpness and peak position with a low-angle $00l$ reflection corresponding to the lamellar stacking of the QPs (see the Supporting Information in refs 11g and 28). The lattice parameters extracted from the XRD data, $a = 3.71$ Å and $c = 6.22$ Å, were contracted relative to the bulk values by 2.7% and 0.2%, respectively (Table 2).

TEM images revealed platelets stacking together vertically and interlinked laterally to adjacent platelets through corners and edges (Figures 10b and S8 in the SI). The lateral fusions led to lacy (Figure 10b) and rough ribbon morphologies (Figure S8a in the SI) of interconnected platelets. The rectangular platelet dimensions were approximately 100 nm × 100 nm. Zebra-striped patterns were evident in some images (Figure S8b in the SI), which may have been due to edge views of vertically stacked platelets or to ZnS lattice fringes.

ZnSe QPs. Nanoclusters of ZnSe were synthesized in an *n*-octylamine–di-*n*-octylamine cosolvent mixture to facilitate their conversion to ZnSe QPs. In the cosolvent mixture, the QPs

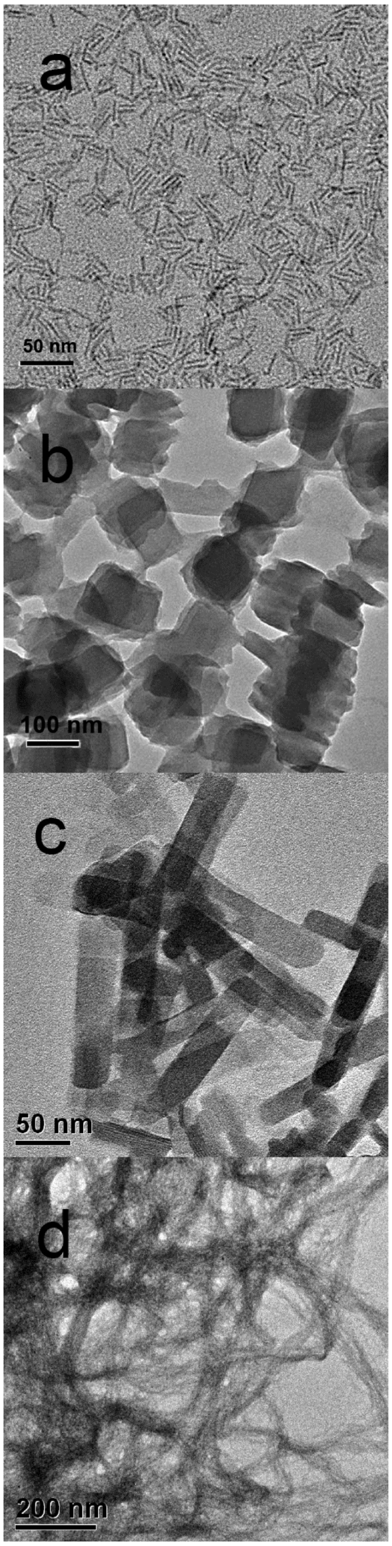

Figure 10. TEM images of (a) CdS QPs, (b) ZnS QPs, (c) ZnSe QPs, and (d) CdTe quantum belts.

were observed to form at 100 °C, whereas their formation in a primary-amine cosolvent required 170 °C.[29] Reaction monitoring by absorption spectroscopy established the intermediacy of nanoclusters larger than the amine-ligated $(ZnSe)_{13}$ derivatives characterized above. A spectrum obtained early in the synthesis (after 2 h) contained three absorptions at 313, 294, and 280 nm (Figure S9 in the SI). The lowest-energy feature was red-shifted relative to that of $(ZnSe)_{13}$ at 289 nm (Table 1) and blue-shifted relative to that of $(CdSe)_{34}$ at 418 nm (Table 1). Moreover, this intermediate spectrum, having a prominent, sharp low-energy feature and two broader higher-energy features, was highly reminiscent of those of the isolated derivatives of $(CdSe)_{34}$, $(CdS)_{34}$, and $(ZnS)_{34}$ (Figures 2 and S2 in the SI). Thus, we strongly suspect that the intermediate nanocluster $(ZnSe)_{34}$, although not yet isolated and fully characterized, was the immediate precursor to the ZnSe QPs.

The absorption spectrum of the ZnSe QPs (Figure 8c) contained two sharp features at 347 and 329 nm, which were assigned to the 1_B-1_e and 1_A-1_e quantum-well transitions. The platelets exhibited wurtzite structures, and the heavy-hole and light-hole bands in wurtzite semiconductors are conventionally labeled B and A, respectively.[30] In this case, the heavy-hole−light-hole splitting in the $n = 1$ quantum-well transition was clearly resolved, as was previously reported for ZnSe nanosheets[29] and thin-film ZnSe quantum wells.[31] A third, higher-lying absorption at 304 nm, if real, would be assigned to the 2_B-2_e transition.

Our absorption data closely matched those previously reported for wurtzite ZnSe nanosheets prepared at higher temperature.[29] In that prior synthesis, the thickness of the nanosheets was determined to be 1.4 nm. The agreement of the two sets of spectral data indicated that our QPs had the same discrete thickness.

The XRD pattern of the ZnSe QPs (Figure 9c) was also fairly sharp, again likely because of the higher synthesis temperature employed, and was indexed to the wurtzite structure. The lattice parameters $a = 3.88$ Å and $c = 6.45$ Å were contracted relative to the bulk values by 2.5% and 1.3%, respectively (Table 2). TEM images of the platelets (Figure 10c) revealed rectangular morphologies and a comparatively large mean length (170 nm) and mean width (25 nm). These larger dimensions are likely also due to the higher synthesis temperature.

CdTe Quantum Belts. As in the cases described above, CdTe nanoclusters were synthesized in an *n*-octylamine−di-*n*-octylamine cosolvent mixture, in this case using the lamellar $Cd(OAc)_2\cdot 2H_2O$ mesophase, TOPTe, and Super-Hydride as precursors. Quantum belts or nanoribbons of CdTe were obtained at 70 °C. Reaction monitoring by absorption spectroscopy identified a nanocluster intermediate (after 2 h) exhibiting absorptions at 448, 404, and 375 nm (Figure S10 in the SI). These spectral features were readily assignable to a $(CdTe)_{34}$ derivative in a manner analogous to identification of the $(ZnSe)_{34}$ intermediate described above. A comparison of the intermediate spectrum to that of the $(CdTe)_{13}$ derivatives (Table 1) established it to correspond to a nanocluster of larger size. Additionally, the shape of the spectrum, with its strong, narrow feature at 448 nm and a pair of less-intense features at 404 and 375 nm, was remarkably similar to that of the isolated *n*-octylamine derivative of $(CdSe)_{34}$ (Figure S2c in the SI). As expected, the spectral features of $(CdTe)_{34}$ were at lower energies than those of both $(CdSe)_{34}$ (Table 1) and $(ZnTe)_{34}$ (see above). This $(CdTe)_{34}$ intermediate, the apparent precursor to the CdTe quantum belts, remains to be isolated and fully characterized.

The absorption spectrum of the CdTe quantum belts (nanoribbons, Figure 8d) exhibited well-resolved features at 491 and 404 nm, respectively, assigned to the heavy-hole 1_B-1_e and light-hole 1_A-1_e quantum-well transitions, as for the ZnSe quantum belts (see above). Nanoplatelets of zinc-blende CdTe, which have electronic structures nearly identical with our CdTe quantum belts, were previously studied by Dubertret and co-workers.[20b,32] The absorption features in Figure 8d were within a few nanometers of those reported by Dubertret and co-workers for CdTe nanoplatelets having a discrete thickness of 1.9 nm.[32] We surmised that our quantum belts had the same thickness.

As in all of the preceding examples, the XRD pattern of the CdTe quantum belts indexed to a wurtzite structure (Figure 9d). Interestingly, bulk CdTe under standard conditions exists only in the zinc-blende structure, although wurtzite CdTe has been grown as thin films.[33] The lattice parameters $a = 4.27$ Å and $c = 7.24$ Å were contracted relative to the thin-film values[33] by 6.5% and 2.7%, respectively (Table 2). Clear, high-magnification TEM images of the CdTe nanocrystals could not be obtained because of their extreme electron-beam sensitivity. A lower-magnification image of bundled CdTe quantum belts is given in Figure 10d, which established the long lengths of the nanocrystals in comparison to the others reported here.

Attempts To Prepare ZnTe QPs or Quantum Belts. All attempts to prepare ZnTe nanocrystals from ZnTe nanocluster precursors failed. The nanoclusters appeared to be unreactive in the range of 120−150 °C but gave poorly characterizable reaction products at higher temperatures. Absorption features assignable to flat, colloidal nanocrystals were not observed. We suspect that the lamellar mesophase templates were unstable at the high temperatures required to achieve reactivity.

■ DISCUSSION

As noted in the Introduction, several compositions of magic-size CdSe nanoclusters were determined by Kasuya and co-workers to be $(CdSe)_{13}$, $(CdSe)_{19}$, $(CdSe)_{33}$, and $(CdSe)_{34}$ using mass spectrometry.[11d] In the same study, they also observed prominent mass-spectral features for $(CdS)_{13}$, $(CdS)_{33}$, $(CdS)_{34}$, $(ZnS)_{13}$, $(ZnS)_{33}$, and $(ZnS)_{34}$. The 1:1 $(II-VI)_x$ stoichiometries of these nanoclusters contrast with the *non*stoichiometric II−VI compositions of nanoclusters prepared by solution chemistry and crystallographically characterized.[15] These isolated, condensed-phase nanoclusters may be enriched in either II−VI element. Those reported by Owen and co-workers are enriched in the group-II metal cation,[15b,c] such that the II−VI ratios are in the range of 1.25−1.75. Additionally, the nonstoichiometric nanoclusters are stabilized by anionic ligands and exhibit close-packed (generally) zinc-blende core structures. Clearly, these nanoclusters represent a family different from that of the stoichiometric, fullerene-like (cage-like)[16b] magic-size nanoclusters identified by Kasuya.

As previously noted, recent work in our laboratory and that of Sardar and co-workers has resulted in the solution-phase synthesis and isolation of amine-stabilized derivatives of the magic-size nanoclusters $(CdSe)_{13}$[11e,h] and $(CdSe)_{34}$.[11f,g] These purified, single-size derivatives, such as $[(CdSe)_{13}(n\text{-octylamine})_{13}]$[11e] and $[(CdSe)_{34}(n\text{-octylamine})_{16}(\text{di-}n\text{-pentylamine})_2]$,[11g] were characterized by a battery of techniques, including extensive elemental analyses, a comparison of their absorption spectra to theoretical predictions, and LDI mass spectrometry and laser-power-dependent LDI mass spectrometry. These nanoclusters contain no anionic ligands and have 1:1 Cd:Se stoichiometries. The evidence establishing that they are ligated analogues of Kasuya's stoichiometric magic-size CdSe nanoclusters is strong. However, there have not yet been

DOI: 10.1021/ic502637q
Inorg. Chem. 2015, 54, 1165−1177

crystallographic structure determinations of the stoichiometric II–VI nanoclusters, which remain important goals.

Elemental analyses of the five new amine-ligated magic-size II–VI nanoclusters isolated here firmly establish their compositions. As for the CdSe analogues above, they contain no anionic ligands and exhibit 1:1 II–VI stoichiometries. The $(II-VI)_{13}$ derivatives $[(ZnSe)_{13}(n\text{-butylamine})_{13}]$, $[(CdTe)_{13}(n\text{-propylamine})_{13}]$, and $[(ZnTe)_{13}(n\text{-butylamine})_{13}]$ possess the same ligand stoichiometries as the previously characterized[11h] $[(CdSe)_{13}(RNH_2)_{13}]$ derivatives, corresponding to one amine ligand for each group-II atom on the presumed nanocluster cage.[16b] The new $(II-VI)_{34}$ derivative $[(CdS)_{34}(n\text{-butylamine})_{18}]$ exhibits the same ligand stoichiometry as $[(CdSe)_{34}(n\text{-octylamine})_{16}(\text{di-}n\text{-pentylamine})_2]$ does.[11g] The new $(II-VI)_{34}$ derivative $[(ZnS)_{34}(n\text{-butylamine})_{34}]$ possesses a 1:1 ligand-to-Zn ratio, presumably reflecting the higher Lewis acidity of Zn relative to Cd, and the greater strength of the hard acid–hard base interactions between Zn and the primary-amine ligands. Elemental analysis does not determine that the new derivatives have been isolated in single $(II-VI)_x$ sizes or establish what those sizes are. We suggest that absorption spectroscopy provides the best evidence of the nanocluster size.

The absorption-spectral profiles of the new $(II-VI)_{13}$ and $(II-VI)_{34}$ derivatives, including the numbers, patterns, and relative intensities of the absorption features, are remarkably similar to those of the corresponding, previously known, amine-ligated $(CdSe)_{13}$ and $(CdSe)_{34}$ analogues. As described in the Results section, the absorption spectra of the $(CdSe)_{13}$ derivatives (Figure S2a in the SI) contain a closely spaced doublet-like feature that is paralleled in the absorption spectra of the ligated $(ZnSe)_{13}$, $(CdTe)_{13}$, and $(ZnTe)_{13}$ derivatives reported here (Figure 5). These features are energetically shifted relative to one another in the manner consistent with the ordering of the bulk band gaps of the corresponding II–VI semiconductors.

The absorption spectrum of amine-ligated $(CdSe)_{34}$ contains a sharp, intense, lowest-energy feature, and two less-intense higher-energy features (Figure S2b,c in the SI). In some ligand–shell environments, only one of the higher-energy absorptions is resolved (Figure S2b in the SI). The spectrum of the *n*-octylamine derivative of $(CdS)_{34}$ contains two such features (Figure 2a), matching the profile of the $(CdSe)_{34}$ spectra, but the features are shifted to higher energy, as expected, and the third absorbance is apparently shifted under solvent absorbance. The spectrum of $[(ZnS)_{34}(n\text{-butylamine})_{34}]$ is shifted even higher in energy, as expected, and only the sharp, intense lowest-energy feature is observed (Figure 2b). In contrast, the spectra of the ligated $(ZnSe)_{34}$ (Figure S9 in the SI) and $(CdTe)_{34}$ (Figure S10 in the SI) intermediates are sufficiently red-shifted because of their compositions, in which all three of the expected spectral features are observed. The spectrum of $(CdTe)_{34}$ is particularly striking in its similarity to that of the *n*-octylamine derivative of $(CdSe)_{34}$ (Figure S2c in the SI).

The strong resemblance of the absorption spectra of the $(II-VI)_{13}$ and $(II-VI)_{34}$ derivatives reported here to those of the previously characterized amine-ligated $(CdSe)_{13}$ and $(CdSe)_{34}$ nanoclusters suggests that we have assigned their sizes correctly. In all cases, the absorption spectra are comparatively sharp and well-resolved, and no minor or impurity features are observed that could be ascribed to nanoclusters of other sizes. The new $(II-VI)_{13}$ and $(II-VI)_{34}$ nanoclusters appear to be spectroscopically pure.

We have also characterized three of the new magic-size nanoclusters by LDI mass spectrometry. This method is not universally accepted for analyzing the nanocluster speciation in a synthetic sample because fragmentation patterns may not be distinguishable from the speciation initially present and because the high excitation energies involved are believed to be capable of equilibrating the speciation prior to analysis.[15b,34] Indeed, the mass-spectral peak intensities and fragmentation patterns initially reported by Kasuya and co-workers for nanocluster specimens and the bulk semiconductors were closely similar, strongly suggesting equilibration.[11d]

Even so, we find that the mass spectra obtained from various magic-size CdSe nanocluster preparations differ markedly,[11d,e,g] giving distinct masses at high peak intensities for $(CdSe)_{13}$ and $(CdSe)_{34}$ nanoclusters, respectively, indicating that equilibration is far from complete under the appropriate mass-spectral conditions. Moreover, Sardar and co-workers demonstrated, from LDI mass spectra obtained at various laser-power levels, that lower-mass peaks present in the spectra of isolated $(CdSe)_{34}$ were indeed fragment ions and not due to species equilibration within the samples.[11f] In the LDI mass spectra of *n*-butylamine derivatives of $(CdS)_{34}$ (Figure 3a) and $(ZnS)_{34}$ (Figure 3b) and the *n*-octylamine derivative of $(ZnSe)_{13}$ (Figure 6) reported here, prominent peaks are observed corresponding to $(CdS)_{34}$, $(ZnS)_{34}$, and $(ZnSe)_{13}$, respectively, which are at least consistent with the assignments made above on the basis of absorption spectroscopy.

The results provided here and elsewhere show that solution-based syntheses are now capable of producing both stoichiometric (Kasuya-like)[11d] and nonstoichiometric (Owen-like)[15c] II–VI nanoclusters. The interrelationships of these two nanocluster types are presently not understood. Their differing stoichiometries may (potentially) be ascribed to the differences in the synthetic conditions employed. However, representatives from the two families often appear to have very similar absorption spectra. For example, the stoichiometric $[(CdSe)_{13}(\text{primary amine})_{13}]$ nanoclusters exhibit spectral features (at 334–338 and 349–351 nm) that are essentially indistinguishable from those of the nonstoichiometric $[Cd_{35}Se_{20}(O_2CPh)_{30}(n\text{-}C_4H_9NH_2)_{30}]$ nanocluster (at 333 and 350 nm).[15c] Whether these spectral similarities are adventitious or the different nanoclusters interconvert to common solution species has not yet been resolved.

Magic-size nanoclusters of four of the five stoichiometric compositions reported here are shown to be nanocrystal precursors to CdS, ZnS, ZnSe, and CdTe QPs or quantum belts. Amine-ligated $(ZnTe)_{13}$, despite its significant environmental sensitivity, in our hands appears to be thermally unreactive under the conditions applied to the other nanocrystal preparations described here. In all of the other cases, $(II-VI)_{34}$ nanoclusters appear to be the immediate nanocrystal precursors. The ligated derivatives of $(CdS)_{34}$ and $(ZnS)_{34}$ appear to be the stable sizes for those compositions; we have not detected spectral features that may be assigned to either $(CdS)_{13}$ or $(ZnS)_{13}$ for those systems.

The synthesis of *crystalline* CdS QPs from $(CdS)_{34}$ at the very low temperature of 0 °C is a remarkable result and is comparable to the synthesis of CdSe QPs from $(CdSe)_{34}$ at room temperature.[11g] Nanocrystal syntheses are generally conducted at temperatures near or above 200 °C. For comparison, the carboxylate-ligated zinc-blende CdS nanoplatelets reported by Dubertret and co-workers[20b] and Peng and co-workers[20a] were prepared at 180–235 and 170–250 °C, respectively. Our low-temperature synthesis is a demonstration of the facility of magic-size-nanocluster precursors to dramatically lower crystal-nucleation barriers and support low-temperature crystal growth.

We note that none of the nanocrystal syntheses reported here has been optimized or fully explored. Indeed, several superior syntheses, from other laboratories, of flat colloidal nanocrystals of the same compositions are cited in the Results section. Our results serve to demonstrate the utility of the magic-size II–VI nanoclusters as nanocrystal precursors. Given their ease of synthesis as described here, their precisely stoichiometric (1:1 II/VI) compositions, and their labile ligation, we suggest that these nanocluster precursors may have great promise as molecular inks for low-cost semiconductor fabrication.[35]

■ OUTLOOK

In our assessment, the stoichiometric magic-size II–VI nanocluster field is currently at a developmental stage quite analogous to that of the Zintl-ion cluster field just prior to Corbett's seminal advances.[5,6] His discovery of a cation-sequestering strategy enabled the structure determinations of those clusters. Clearly, that is an essential next step for the development of the magic-size II–VI nanocrystal field. We note that these amine-ligated II–VI nanoclusters undergo facile ligand exchange, and so it should soon be possible for us or others to obtain crystallizable derivatives. We expect that the new, discretely sized, magic-size nanoclusters reported here will support further advances in the understanding of the structures, physical properties, and reactivity of this exciting new family of molecular clusters.

■ ASSOCIATED CONTENT

Ⓢ Supporting Information

Plots of the measured basal-plane *d* spacing, additional UV–visible absorption spectra, spectral evolution upon transformation, and additional TEM data. This material is available free of charge via the Internet at http://pubs.acs.org.

■ AUTHOR INFORMATION

Corresponding Author

*E-mail: buhro@wustl.edu.

Notes

The authors declare no competing financial interest.

■ ACKNOWLEDGMENTS

This work was supported by the NSF under Grant CHE-1306507. We thank Professor Richard Loomis (Washington University) for helpful discussions.

■ REFERENCES

(1) Lipscomb, W. N. *J. Chem. Phys.* **1954**, *22*, 985–988.

(2) Casanova, J. *The Borane, Carborane, Carbocation Contiuum*; John Wiley & Sons, Inc.: New York, 1998.

(3) Housecroft, C. E. *Boranes and metallaboranes*; Ellis Horwood Ltd.: Herts, U.K., 1994.

(4) Rudolph, R. W. *Acc. Chem. Res.* **1976**, *9*, 446–452.

(5) Corbett, J. D. *Chem. Rev.* **1985**, *85*, 383–397.

(6) Corbett, J. D.; Adolphson, D. G.; Merryman, D. J.; Edwards, P. A.; Armatis, F. J. *J. Am. Chem. Soc.* **1975**, *97*, 6267–6268.

(7) Kräetschmer, W.; Lamb, L. D.; Fostiropoulos, K.; Huffman, D. R. *Nature* **1990**, *347*, 354–358.

(8) Curl, R. F.; Smalley, R. E. *Sci. Am.* **1991**.

(9) Lu, X.; Bao, L.; Akasaka, T.; Nagase, S. *Chem. Commun.* **2014**, *50*, 14701–14715.

(10) Vostrowsky, O.; Hirsch, A. *Chem. Rev.* **2006**, *106*, 5191–5207.

(11) (a) Kudera, S.; Zanella, M.; Giannini, C.; Rizzo, A.; Li, Y. Q.; Gigli, G.; Cingolani, R.; Ciccarella, G.; Spahl, W.; Parak, W. J.; Manna, L. *Adv. Mater.* **2007**, *19*, 548–552. (b) Dukes, A. D.; McBride, J. R.; Rosenthal, S. J. *Chem. Mater.* **2010**, *22*, 6402–6408. (c) Noda, Y.; Maekawa, H.; Kasuya, A. *Eur. Phys. J. D* **2010**, *57*, 43–47. (d) Kasuya, A.; Sivamohan, R.; Barnakov, Y. A.; Dmitruk, I. M.; Nirasawa, T.; Romanyuk, V. R.; Kumar, V.; Mamykin, S. V.; Tohji, K.; Jeyadevan, B.; Shinoda, K.; Kudo, T.; Terasaki, O.; Liu, Z.; Belosludov, R. V.; Sundararajan, V.; Kawazoe, Y. *Nat. Mater.* **2004**, *3*, 99–102. (e) Wang, Y.; Liu, Y. H.; Zhang, Y.; Wang, F.; Kowalski, P. J.; Rohrs, H. W.; Loomis, R. A.; Gross, M. L.; Buhro, W. E. *Angew. Chem., Int. Ed.* **2012**, *51*, 6154–6157. (f) Dolai, S.; Nimmala, P. R.; Mandal, M.; Muhoberac, B. B.; Dria, K.; Dass, A.; Sardar, R. *Chem. Mater.* **2014**, *26*, 1278–1285. (g) Wang, Y.; Zhang, Y.; Wang, F.; Giblin, D. E.; Hoy, J.; Rohrs, H. W.; Loomis, R. A.; Buhro, W. E. *Chem. Mater.* **2014**, *26*, 2233–2243. (h) Wang, Y.; Liu, Y. H.; Zhang, Y.; Kowalski, P. J.; Rohrs, H. W.; Buhro, W. E. *Inorg. Chem.* **2013**, *52*, 2933–2938.

(12) Fojtik, A.; Weller, H.; Koch, U.; Henglein, A. *Ber. Bunsenges. Phys. Chem.* **1984**, *88*, 969–977.

(13) (a) Liu, Y. H.; Wang, F. D.; Wang, Y. Y.; Gibbons, P. C.; Buhro, W. E. *J. Am. Chem. Soc.* **2011**, *133*, 17005–17013. (b) Yu, J. H.; Liu, X.; Kweon, K. E.; Joo, J.; Park, J.; Ko, K. T.; Lee, D. W.; Shen, S. P.; Tivakornsasithorn, K.; Son, J. S.; Park, J. H.; Kim, Y. W.; Hwang, G. S.; Dobrowolska, M.; Furdyna, J. K.; Hyeon, T. *Nat. Mater.* **2009**, *9*, 47–53.

(14) Peng, Z. A.; Peng, X. *J. Am. Chem. Soc.* **2002**, *124*, 3343–3353.

(15) (a) Lee, G. S.; Craig, D. C.; Ma, I.; Scudder, M. L.; Bailey, T. D.; Dance, I. G. *J. Am. Chem. Soc.* **1988**, *110*, 4863–4864. (b) Cossairt, M.; Owen, J. S. *Chem. Mater.* **2011**, *23*, 3114–3119. (c) Beecher, A. N.; Yang, X.; Palmer, J. H.; LaGrassa, A. L.; Juhas, P.; Billings, S. J. L.; Owen, J. S. *J. Am. Chem. Soc.* **2014**, *136*, 10645–10653. (d) Soloviev, V. N.; Eichhofer, A.; Fenske, D.; Banin, U. *J. Am. Chem. Soc.* **2001**, *123*, 2354–2364. (e) Herron, N.; Calabrese, J. C.; Farneth, W. E.; Wang, Y. *Science* **1993**, *259*, 1426–8. (f) Soloviev, V. N.; Eichhofer, A.; Fenske, D.; Banin, U. *J. Am. Chem. Soc.* **2000**, *122*, 2673–2674.

(16) (a) Del Ben, M.; Havenith, R. W. A.; Broer, R.; Stener, M. *J. Phys. Chem. C* **2011**, *115*, 16782–16796. (b) Nguyen, K. A.; Day, P. N.; Pachter, R. *J. Phys. Chem. C* **2010**, *114*, 16197–16209. (c) Singh, T.; Mountziaris, T. J.; Maroudas, D. *Appl. Phys. Lett.* **2012**, *100*, 053105.

(17) Son, J. S.; Wen, X. D.; Joo, J.; Chae, J.; Baek, S.; Park, K.; Kim, J. H.; An, K.; Yu, J. H.; Kwon, S. G.; Choi, S. H.; Wang, Z.; Kim, Y. W.; Kuk, Y.; Hoffmann, R.; Hyeon, T. *Angew. Chem., Int. Ed.* **2009**, *48*, 6861–6864.

(18) (a) Ikawa, N.; O, Y.; Kimura, T. *J. Mater. Sci.* **2008**, *43*, 4198–4207. (b) Kitaigorodsky, A. I. *Molecular crystals and molecules*; Academic Press: New York, 1973.

(19) Zhang, J.; Jin, S.; Fry, H. C.; Peng, S.; Shevchenko, E.; Wiederrecht, G. P.; Rajh, T. *J. Am. Chem. Soc.* **2011**, *133*, 15324–15327.

(20) (a) Li, Z.; Qin, H.; Guzun, D.; Benamara, M.; Salamo, G.; Peng, X. *Nano Res.* **2012**, *5*, 337–351. (b) Ithurria, S.; Tessier, M. D.; Mahler, B.; Lobo, R. P. S. M.; Dubertret, B.; Efros, A. L. *Nat. Mater.* **2011**, *10*, 936–941.

(21) Wang, F.; Wang, Y.; Liu, Y. H.; Morrison, P. J.; Loomis, R. A.; Buhro, W. E. *Acc. Chem. Res.* **2014**, Articles ASAP.

(22) Madelung, O. *Semiconductors Data Handbook*; Springer: New York, 2004.

(23) Son, J. S.; Park, K.; Kwon, S. G.; Yang, J.; Choi, M. K.; Kim, J.; Yu, J. H.; Joo, J.; Hyeon, T. *Small* **2012**, *8*, 2394–2402.

(24) Yu, S. H.; Yang, J.; Qian, Y. T.; Yoshumura, M. *Chem. Phys. Lett.* **2002**, *361*, 362–366.

DOI: 10.1021/ic502637q
Inorg. Chem. 2015, 54, 1165–1177

(25) Li, J.; Xu, Y.; Wei, W.; Wu, D.; Sun, Y. *Colloids Surf. A* **2006**, *287*, 222−225.

(26) (a) Kole, A. K.; Tiwary, C. S.; Kumbhakar, P. *CrystEngComm* **2013**, *15*, 5515−5525. (b) Srinivasan, N.; Thirumaran, S.; Ciattini, S. *Spectrochim. Acta, Part A* **2013**, *102*, 253−268.

(27) Liu, Y. H.; Wayman, V. L.; Gibbons, P. C.; Loomis, R. A.; Buhro, W. E. *Nano Lett.* **2010**, *10*, 352−357.

(28) Morrison, P. J.; Loomis, R. A.; Buhro, W. E. *Chem. Mater.* **2014**, *26*, 5012−5019.

(29) Park, H.; Chung, H.; Kim, W. *Mater. Lett.* **2013**, *99*, 172−175.

(30) Madelung, O. *Semiconductors-Basic Data*; Springer: Berlin, 1996.

(31) (a) Seemann, M.; Kieseling, F.; Stolz, H.; Manzke, G.; Henneberger, K.; Passow, T.; Hommel, D. *Phys. Status Solidi* **2006**, *3*, 2453−2456. (b) Lee, C. D.; Min, S. I.; Chang, S. K. *J. Cryst. Growth* **1996**, *159*, 108−111. (c) Coquillat, D.; Hamdani, F.; Lasaray, J. P.; Briot, O.; Aulombard, R. L. *Phys. Rev. B* **1993**, *47*, 10489−10496. (d) Papageorgiou, G.; Chari, R.; Brown, G.; Kar, A. K.; Bradford, C.; Prior, K. A.; Kalt, H.; Galbraith, I. *Phys. Rev. B* **2004**, *69*, 085311-1−085311-5.

(32) Pedetti, S.; Nadal, B.; Lhuillier, E.; Mahler, B.; Bouet, C.; Abecassis, B.; Xu, X.; Dubertret, B. *Chem. Mater.* **2013**, *25*, 2455−2462.

(33) Weinstein, M.; Wolff, G.; Das, B. N. *Appl. Phys. Lett.* **1965**, *6*, 73−75.

(34) Evans, C. M.; Love, A. M.; Weiss, E. A. *J. Am. Chem. Soc.* **2012**, *134*, 17928−17305.

(35) (a) Mitzi, D. B. *Adv. Mater.* **2009**, *21*, 3141−3158. (b) Habas, S. E.; Platt, H. A. S.; van Hest, M. F. A. M.; Ginley, D. S. *Chem. Rev.* **2010**, *110*, 6571−6594.